CGILS: Results from the first phase of an international project to understand the physical mechanisms of low cloud feedbacks in single column models

Minghua Zhang,[1] Christopher S. Bretherton,[2] Peter N. Blossey,[2] Phillip H. Austin,[3] Julio T. Bacmeister,[4] Sandrine Bony,[5] Florent Brient,[5] Suvarchal K. Cheedela,[6] Anning Cheng,[7] Anthony D. Del Genio,[8] Stephan R. De Roode,[9] Satoshi Endo,[10] Charmaine N. Franklin,[11] Jean-Christophe Golaz,[12] Cecile Hannay,[4] Thijs Heus,[6] Francesco Alessandro Isotta,[13] Jean-Louis Dufresne,[5] In-Sik Kang,[14] Hideaki Kawai,[15] Martin Köhler,[16] Vincent E. Larson,[17] Yangang Liu,[10] Adrian P. Lock,[18] Ulrike Lohmann,[13] Marat F. Khairoutdinov,[1] Andrea M. Molod,[19] Roel A. J. Neggers,[20] Philip Rasch,[21] Irina Sandu,[6,16] Ryan Senkbeil,[17] A. Pier Siebesma,[20] Colombe Siegenthaler-Le Drian,[13] Bjorn Stevens,[6] Max J. Suarez,[19] Kuan-Man Xu,[7] Knut von Salzen,[22] Mark J. Webb,[18] Audrey Wolf,[23] and Ming Zhao[12]

[1] CGILS—the CFMIP-GASS Intercomparison of Large Eddy Models (LESs) and single column models (SCMs)—investigates the mechanisms of cloud feedback in SCMs and LESs under idealized climate change perturbation. This paper describes the CGILS results from 15 SCMs and 8 LES models. Three cloud regimes over the subtropical oceans are studied: shallow cumulus, cumulus under stratocumulus, and well-mixed coastal stratus/stratocumulus. In the stratocumulus and coastal stratus regimes, SCMs without activated shallow convection generally simulated negative cloud feedbacks, while models with active shallow convection generally simulated positive cloud feedbacks. In the shallow cumulus alone regime, this relationship is less clear, likely due to the changes in cloud depth, lateral mixing, and precipitation or a combination of them. The majority of LES models simulated negative cloud feedback in the well-mixed coastal stratus/stratocumulus regime, and positive feedback in the shallow cumulus and stratocumulus regime. A general framework is provided to interpret SCM results: in a warmer climate, the moistening rate of the cloudy layer associated with the surface-based turbulence parameterization is enhanced; together with weaker

[1]School of Marine and Atmospheric Sciences, Institute for Terrestrial and Planetary Atmospheres, Stony Brook University, Stony Brook, New York, USA.

[2]Department of Atmospheric Sciences, University of Washington, Seattle, Washington, USA.

[3]Department of Earth and Ocean Science, University of British Columbia, Vancouver, British Columbia, Canada.

[4]National Center for Atmospheric Research, Earth System Laboratory, Boulder, Colorado, USA.

[5]Laboratoire de Meteorologie Dynamique/Institute Pierre Simon Laplace (IPSL), Paris, France.

[6]Max Planck Institute for Meteorology, Hamburg, Germany.

[7]NASA Langley Research Center, Hampton, Virginia, USA.

[8]NASA Goddard Institute for Space Studies, New York, New York, USA.

[9]Department of Geoscience & Remote Sensing, Delft University of Technology, Delft, Netherlands.

[10]Brookhaven National Laboratory, Environmental Sciences Department, Upton, New York, USA.

[11]Centre for Australian Weather and Climate Research, Commonwealth Scientific and Industrial Research Organisation (CSIRO), Aspendale, Victoria, Australia.

[12]NOAA Geophysical Fluid Dynamics Laboratory, Princeton, New Jersey, USA.

[13]Swiss Federal Institute of Technology, Zurich, Switzerland.

[14]School of Earth and Environmental Sciences, Seoul National University, Seoul, South Korea.

[15]Meteorological Research Institute, Tsukuba, Japan.

[16]European Centre for Medium-Range Weather Forecasts, Reading, UK.

[17]Department of Mathematical Sciences, University of Wisconsin, Milwaukee, Wisconsin, USA.

[18]Met Office Hadley Centre, Exeter, UK.

[19]Global Modeling and Assimilation Office, NASA Goddard Space Flight Center, Greenbelt, Maryland, USA.

[20]Atmospheric Research Division, Royal Netherlands Meteorological Institute (KNMI), De Bilt, Netherlands.

[21]Pacific Northwest National Laboratory, Richland, Washington, USA.

[22]Canadian Centre for Climate Modelling and Analysis, Victoria, British Columbia, Canada.

[23]Goddard Institute for Space Studies, Columbia University, New York, New York, USA.

Corresponding author: M. Zhang, School of Marine and Atmospheric Sciences, Institute for Terrestrial and Planetary Atmospheres, Stony Brook University, Stony Brook, NY 11794-5000, USA. (minghua.zhang@stonybrook.edu)

large-scale subsidence, it causes negative cloud feedback. In contrast, in the warmer climate, the drying rate associated with the shallow convection scheme is enhanced. This causes positive cloud feedback. These mechanisms are summarized as the "NESTS" negative cloud feedback and the "SCOPE" positive cloud feedback (Negative feedback from Surface Turbulence under weaker Subsidence—Shallow Convection PositivE feedback) with the net cloud feedback depending on how the two opposing effects counteract each other. The LES results are consistent with these interpretations.

1. Introduction

[2] Cloud-climate feedbacks in General Circulation Models (GCMs) have been the subject of intensive study for the last four decades [e.g., *Randall et al.*, 2007]. These feedbacks were identified to be one of the most significant uncertainties in projecting future global warming in past IPCC (Inter-Governmental Panel for Climate Change) Assessment Reports (AR), as well as in coupled model simulations that will be used for the upcoming AR5 [*Andrews et al.*, 2012]. Despite much progress toward understanding cloud feedbacks [*Bony et al.*, 2006], however, there is still a general lack of knowledge about their mechanisms. Understanding the physical mechanisms is necessary to increase our confidence in the sensitivity estimates of climate models.

[3] Cloud-climate feedbacks refer to the radiative impact of changes of clouds on climate change. Because clouds are not explicitly resolved in GCMs, they are the product of an interactive and elaborate suite of physical parameterizations. As a result, it has been a challenge to decipher cloud feedback mechanisms in climate models. Clouds also interact with the resolved-scale atmospheric dynamical circulations through their impact on latent and radiative heating.

[4] In view of the challenges, CFMIP (the Cloud Feedback Model Intercomparison Project) and GASS (Global Atmospheric System Studies) initiated a joint project—CGILS (the CFMIP-GASS Intercomparison of Large Eddy Models (LESs) and single column models (SCMs)) to analyze the physical mechanisms of cloud feedbacks in SCMs by using an idealized experimental setup. The focus of CGILS is on low clouds in the subtropics, because several studies have demonstrated that these clouds contribute significantly to cloud feedback differences in models [e.g., *Bony and Dufresne*, 2005; *Zelinka et al.*, 2012]. The role played by these clouds is consistent with the fact that low clouds have the largest net cloud-radiative effect, in contrast to deep clouds in which the positive longwave and negative shortwave cloud effects largely cancel out [e.g., *Ramanathan et al.*, 1989].

[5] The objective of this paper is to describe the CGILS project and results from 15 SCMs and 8 LES models. Section 2 briefly describes the experimental design and large-scale forcing data. Section 3 gives a brief description of the participating models. Section 4 discusses simulated clouds and the associated physical processes. Section 5 presents cloud feedback results. A brief summary is given in Section 6.

2. Experimental Design and Large-Scale Forcing Data

2.1. Experimental Design

[6] The CGILS experimental design was described in *Zhang et al.* [2012], which is schematically shown in Figure 1. In the control climate (CTL), sea surface temperature (SST) is specified along the GCSS/WGNE Pacific Cross Section Intercomparison (GPCI) [*Teixeira et al.*, 2011] in the northeast Pacific by using the ECMWF (European Center for Medium-Range Weather Forecasts) Interim Reanalysis (ERA-Interim) [*Dee et al.*, 2011] July 2003 condition as given in Table 1 of *Zhang et al.* [2012]. In the perturbed climate, SST is uniformly raised everywhere by 2° as in *Cess et al.* [1990]. Large-scale horizontal advection and vertical motion, corresponding to the underlying SST, were derived and used to force SCMs and LES models. The perturbed climate is referred to as P2S, with "S" denotes that the large-scale subsidence is also different from CTL [*Bretherton et al.*, 2013]. The models simulate changes of clouds in response to changes of SST and the associated large-scale atmospheric conditions.
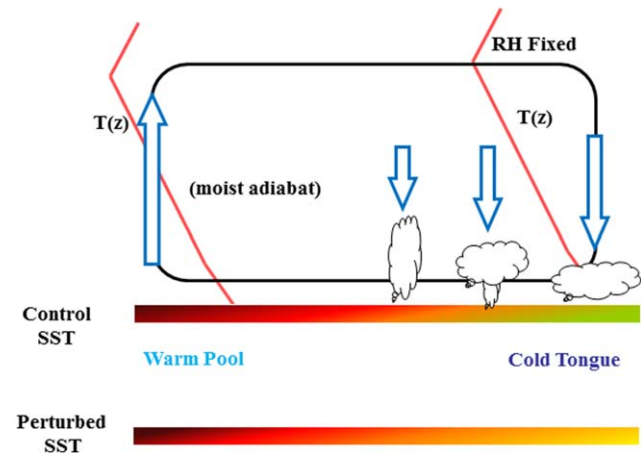

Figure 1. Schematics of the experimental setup. The atmospheric temperature and water vapor are constructed based on moist adiabat and fixed relative humidity, respectively. The large-scale subsidence is calculated based on the clear-sky thermodynamic equation. These fields change with SST warming of 2°C in the perturbed climate.

Table 1. Participating Models, Main References, and Contributors[a]

Models Acronyms	Model Institution	References	Contributors	Layers: Total/ ($p > 700$ hPa)
SCM (15)				
ACCESS (Australian Community Climate and Earth System Simulator)	Australian Commonwealth Scientific and Industrial Research Organisation/ Centre for Australian Weather and Climate Research	*Hewitt et al.* [2011]	Charmaine Franklin	38/12
CAM4 (Community Atmospheric Model Version 4)	National Center for Atmospheric Research (NCAR), USA	*Neale et al.* [2010]	Minghua Zhang, Cecile Hannay, and Philip Rasch	26/5
CAM5 (Community Atmospheric Model Version 4)	National Center for Atmospheric Research (NCAR), USA	*Neale et al.* [2012]	Minghua Zhang, Cecile Hannay, and Philip Rasch	30/9
CCC (Canadian Centre for Climate)	Canadian Centre for Climate Modelling and Analysis, Canada	*Ma et al.* [2010]	Phillip Austin and Knut von Salzen	35/14
CLUBB (Cloud Layers Unified By Binormals)	University of Wisconsin at Milwaukee, USA	*Golaz et al.* [2002a, 2002], *Larson and Golaz* [2005], and *Golaz et al.* [2007]	Vincent Larson and Ryan Senkbeil	41/29
ECHAM6 (ECMWF- University of Hamburg Model Version 6)	Max-Planck Institute of Meteorology, Germany	*Stevens et al.* [2013]	Suvarchal Cheedela and Bjorn Stevens	31/9
ECMWF (European Center for Medium Range Weather Forecasting)	European Center for Medium Range Weather Forecasting	*Neggers et al.* [2009a, 2009b]	Martin Koehler	91/20
EC-ETH (ECMWF- Eidgenössische Technische Hochschule)	Swiss Federal Institute of Technology, Switzerland	*Isotta et al.* [2011]	Colombe Siegenthaler-Le Drian, Isotta Francesco Alessandro, and Ulrike Lohman	31/9
GFDL-AM3 (Geophysical Fluid Dynamics Laboratory Atmospheric Model Version 3)	NOAA Geophysical Fluid Dynamics Laboratory, USA	*Donner et al.* [2011]	Jean-Christophe Golaz and Ming Zhao	48/12
GISS (Goddard Institute for Space Studies)	NASA Goddard Institute for Space Studies, USA	*Schmidt et al.* [2006]	Anthony DelGenio and Audrey Wolf	40/9
GMAO (NASA Global Modeling and Assimilation Office)	NASA Goddard Space Flight Center, USA	*Rienecker et al.* [2008] and *Molod et al.* [2012]	Andrea Molod, Max Suarez, and Julio Bacmeister	72/13
HadGEM2 (Hadley Centre Global Environment Model version 2)	Met Office, United Kingdom	*Lock et al.* [2001] and *Martin et al.* [2011]	Adrian Lock and Mark Webb	38/12
JMA (Japan Meteorological Agency)	Japan Meteorological Agency, Japan	*Kawai* [2012]	Hideaki Kawai	60/16
IPSL (Institute Pierre Simon Laplace)	Institute Pierre Simon Laplace (IPSL), France	*Hourdin et al.* [2006]	Florent Brient, Sandrine Bony, and Jean-Louis Dufresne	39/12
RACMO (Regional Atmospheric Climate Model)	Royal Netherlands Meteorological Institute, the Netherlands	*Neggers et al.* [2009a, 2009b]	Roel Neggers and Pier Siebesma	91/20
LES (8)				
DALES (Dutch Atmospheric Large-Eddy Simulation)	Royal Netherlands Meteorological Institute, the Netherlands	*Heus et al.* [2010]	Stephan de Roode	
LARC (NASA Langley Research Center)	NASA Langley Research Center, USA	*Xu et al.* [2010]	Anning Cheng and Kuan-man Xu	
SAM (System for Atmospheric Models)	University of Washington/ Stony Brook University, USA	*Khairtoutdinov and Randall* [2003]	Peter Blossey, Chris Bretherton, and Marat Khairoutdinov	
SAMA (System for Atmospheric Models)	University of Washington/ Stony Brook University, USA	*Khairtoutdinov and Randall* [2003] and *Blossey et al.* [2013]	Peter Blossey, Chris Bretherton, and Marat Khairoutdinov	
MOLEM (Met Office Large Eddy Model)	Met Office, United Kingdom	*Lock* [2009]	Adrian Lock	
MOLEMA (Met Office Large Eddy Model)	Met Office, United Kingdom	*Lock* [2009] and *Blossey et al.* [2013]	Adrian Lock	
UCLA (University of California at Los Angeles)	Max Plank Institute of Meteorology, Germany/ University of California at Los Angeles, USA	*Stevens et al.* [2005] and *Stevens and Seifert* [2008]	Thijs Heus, Irina Sandu, and Bjorn Stevens	

Table 1. (continued)

Models Acronyms	Model Institution	References	Contributors	Layers: Total/ ($p > 700$ hPa)
WRF (Weather Research and Forecasting)	National Center for Atmospheric Research/ Brookhaven National Laboratory	*Endo et al.* [2011]	Satosh End and Yangang Liu	

[a]The number of vertical layers and layers between the surface and 700 hPa for SCMs are given in the last column.

[7] Three locations along the GPCI cross section are selected for study. They are labeled as S6, S11, and S12 in Figure 2, which also shows the distribution of low cloud amount in the summer (JJA, June to August) from the merged CALIPSO, CloudSat, CERES, and MODIS satellite product C3M [*Kato et al.*, 2011; *Xu and Cheng*, 2013]. Typical regimes of clouds at these three locations are shallow cumulus (S6), cumulus under stratocumulus (S11), and well-mixed stratocumulus or coastal stratus (S12). On the basis of dominant cloud types, they are referred to as shallow cumulus, stratocumulus, and coastal stratus, respectively. The locations and values of summer-time surface meteorological variables in the control climate can be found in Table 1 of *Zhang et al.* [2012].

2.2. Forcing Data

[8] The SCM and LES forcing data refer to the large-scale horizontal advective tendencies and vertical velocity, and surface boundary conditions that are specified in the model simulations. The SCMs calculate the time evolution of water vapor and temperature as follows [*Randall and Cripe*, 1999]:

$$\frac{\partial \theta_m}{\partial t} = \left(\frac{\partial \theta_m}{\partial t}\right)_{phy} - \left(\vec{V} \cdot \nabla \theta\right)_{LS} - \omega_{LS}\frac{\partial \theta_m}{\partial p}, \quad (1)$$

$$\frac{\partial q_m}{\partial t} = \left(\frac{\partial q_m}{\partial t}\right)_{phy} - \left(\vec{V} \cdot \nabla q\right)_{LS} - \omega_{LS}\frac{\partial q_m}{\partial p}, \quad (2)$$

where θ and q are potential temperature and water vapor mixing ratio. Subscript "m" denotes model calculations; "LS" stands for large-scale; other symbols are as commonly used. The first term on the right-hand side (RHS) of equations (1) and (2) is calculated from physical parameterizations (with subscript "$phys$"). The last two terms contain the specified large-scale horizontal advective forcing and subsidence. In LES models, conservative variables like liquid water potential temperature and total liquid water are typically used as prognostic fields [e.g., *Siebesma et al.*, 2004; *Stevens et al.*, 2005]. Equations (1) and (2) represent domain averages. The atmospheric winds and initial relative humidity are specified by using the ERA-Interim for July 2003. Initial profiles of atmospheric temperature are assumed to follow moist adiabat over the warm pool and weak gradient approximations at other locations [*Sobel et al.*, 2001]. Surface latent and sensible heat fluxes are calculated internally by each model from the specified SST and winds.

[9] The large-scale horizontal advective tendencies and subsidence in equations (1) and (2) are specified according to SST. In the free troposphere, they are derived based on the clear-sky thermodynamic and water vapor mass continuity equations, in which radiative cooling in the thermodynamic equation is balanced by subsidence warming and horizontal advection, with the radiative cooling calculated by using the RRTM radiation code [*Mlawer et al.*, 1997] and the horizontal advection constrained by ERA-Interim. Below the altitude of 900 hPa, the horizontal advective forcing of temperature and water vapor are calculated using the SST spatial gradient and specified surface relative humidity. The detailed derivation of the CGILS forcing data and its comparison with the corresponding GCM and ERA-Interim can be found in *Zhang et al.* [2012].

[10] Figure 3a shows the derived vertical profiles of ω_{LS} in CGILS CTL (solid lines) and ERA-Interim (dashed lines) at the three chosen locations. The obtained values match well with ERA-Interim in the lower troposphere. Among the three locations, the subsidence rate is the strongest at S12 and the weakest at S6.

[11] Figure 3b shows the comparison of the derived ω_{LS} between CTL (solid lines) and P2S (dashed lines) used in the simulations. It is seen that subsidence is weaker in the warmer climate. Figures 3c and 3d show the corresponding profiles of horizontal advective tendencies of temperature and water vapor, respectively. In the free troposphere, these profiles, along with
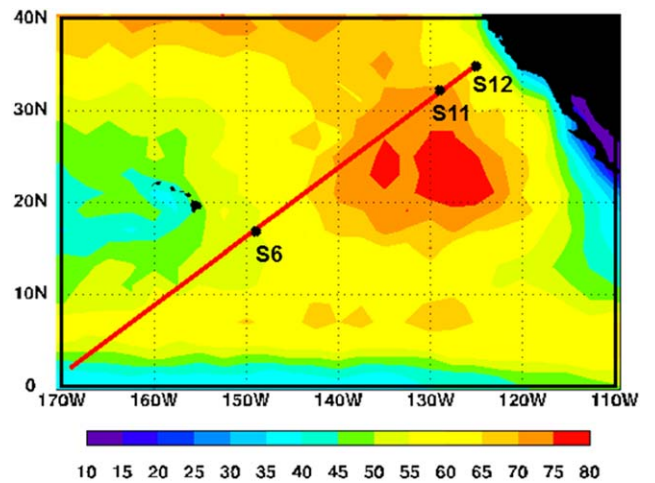

Figure 2. Averaged amount of low clouds in June-July-August (%) from the C3M satellite data. The red line is the northern portion of the GPCI (see text); the symbols "S6," "S11," and "S12" are the three locations studied in the paper.
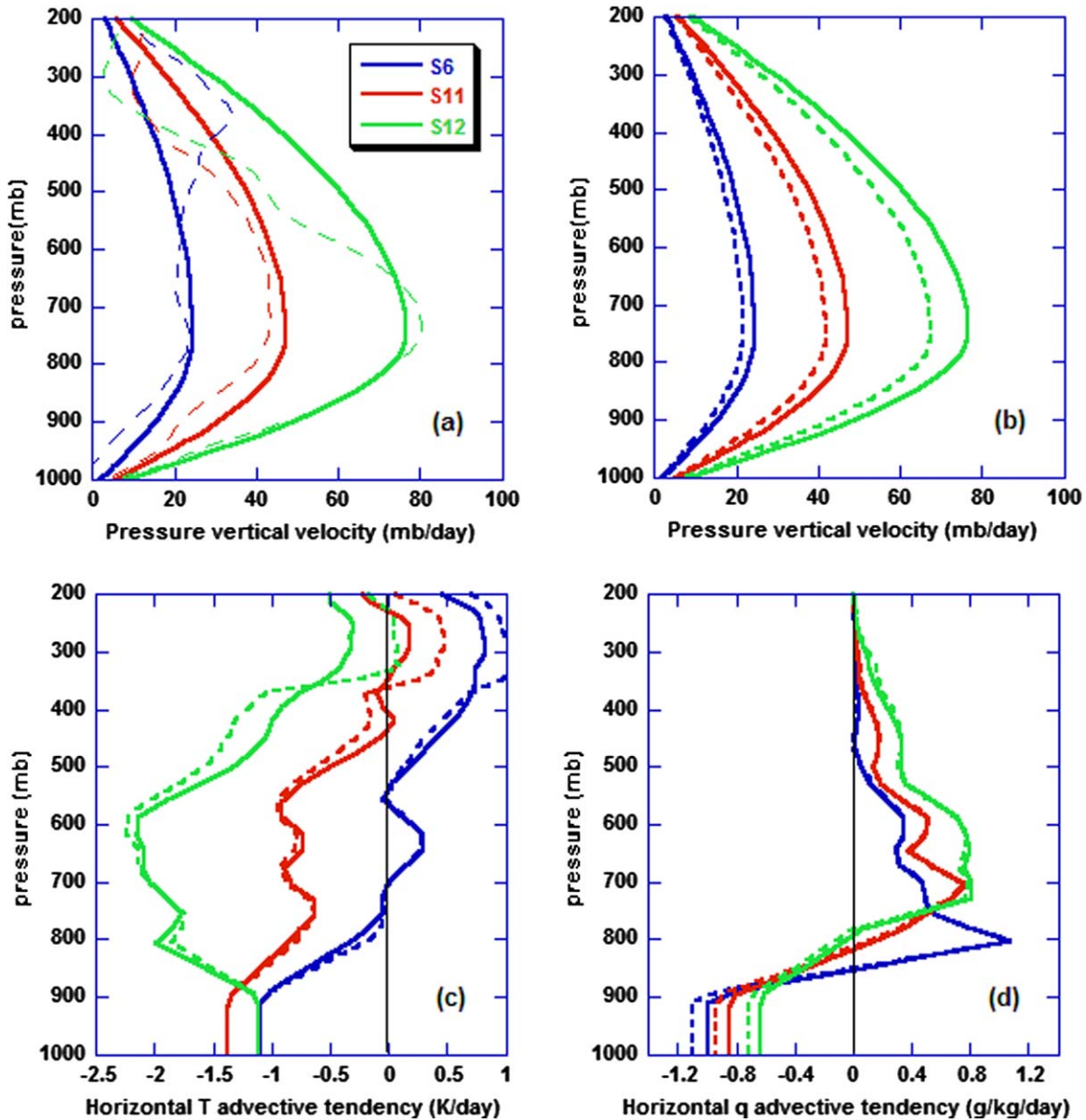
Figure 3. (a) Large-scale pressure vertical velocity at the three locations in the control climate (solid lines), and in the ERA-Interim (dashed). (b) Same as Figure 3a except that the dashed lines denote subsidence rates in the warmer climate. (c) Same as Figure 3b except for horizontal advective tendency of temperature. (d) Same as Figure 3c except for advective tendency of water vapor.

the profiles of ω_{LS}, SST, and initial atmospheric temperature and water vapor, satisfy the clear-sky atmospheric thermodynamic and water vapor mass continuity equations under 15 July insolation conditions. *Zhang et al.* [2012] showed that the changes in the forcing data between CTL and P2S in Figure 3 capture the essential features in GCMs. All data are available at the CGILS website http://atmgcm.msrc.sunysb.edu/cfmip_figs/Case_specification.html.

2.3. Simulations

[12] We use the change of cloud-radiative effect (CRE) from CTL to P2S, as in many previous studies,

to measure cloud feedbacks. Even though *Soden et al.* [2004] suggested other better diagnostics of cloud feedbacks, CRE is used for simplicity, which should not affect the results of this paper.

[13] The SCMs and LES are integrated to quasi-equilibrium states by using the same steady large-scale advective tendencies and subsidence as forcing data. Each model ran six simulations: CTL and P2S at the three locations of S6, S11, and S12. Since the forcing is fixed, a model may eventually drift if its radiative cooling rate in the free atmosphere differs from the rate used in the derivation of the prescribed large-scale subsidence. To prevent models from similar drifting, at

Table 2. Boundary-Layer Turbulence Schemes in SCMs

Models	References	Local K_c	Cloud-top Entrainment	Counter Gradient γ_c
ACCESS	*Lock et al.* [2000]	N	Y	Y
CAM4	*Holtslag and Boville* [1993]	N	N	Y
CAM5	*Bretherton and Park* [2009]	Y	Y	N
CCC	*von Salzen et al.* [2013]	Y	Y	Y
CLUBB	*Golaz et al.* [2002a, 2002], *Larson and Golaz* [2005], and *Golaz et al.* [2007]	N	N	N
ECHAM6	*Stevens et al.* [2012]	Y	N	N
ECMWF	*Neggers et al.* [2009a, 2009b] and *Lock* [2000]	N	Y	Y
EC-ETH	*Brinkop and Roeckner* [1995]	Y	N	N
GFDL-AM3	*Lock et al.* [2000] and *Louis and Geleyn* [1982]	N	Y	N
GISS	*Holtslag and Moeng* [1991] and *Del Genio et al.* [1996]	Y	Y	Y
GMAO	*Lock et al.* [2000] and *Louis and Geleyn* [1982]	N	Y	Y
HadGEM2	*Lock et al.* [2000]	N	Y	Y
JMA	*Mellor and Yamada* [1974] and *Kawai* [2012]	Y	N	N
IPSL	*Hourdin et al.* [2006]	Y	N	Y
RACMO	*Neggers et al.* [2009a, 2009b]	N	Y	Y

pressure less than 600 hPa, temperature and water vapor mixing ratio are relaxed to their initial conditions with a time scale of 3 h. In LES models, they are relaxed at altitudes above 4000 m for S6, 2500 m for S11, and 1200 m for S12, respectively, to reduce computational costs and allow for high vertical resolutions in shallow domains. Some LES models did not complete all six simulations.

[14] Most of the SCMs are integrated for 100 days. Based on a visual inspection of statistical equilibrium, the averages of their last period of about 50 days are used. Most LES simulations reached quasi-equilibrium states after 10 days, in which case the last 2 days are used in the analysis. *Zhang and Bretherton* [2008] analyzed the transient behavior of the Community Atmospheric Model (CAM) under constant forcing and showed that the interaction of different physical parameterization components can create quasi-periodic behaviors of model simulation with time scales longer than a day. Since LES models contain fewer parameterization components, the impact of this type of interactions is reduced, which may explain why LES models reach quasi steady states in shorter time than SCMs. To our knowledge, CGILS is the first LES intercomparion study to investigate clouds by integrating them to quasi-equilibrium states.

3. Models and Differences in Physical Parameterizations

[15] Fifteen SCMs and eight LES models participated in this study. Many parent GCMs of the SCMs also participated in the Coupled Model Intercomparison Project 5 (CMIP5). Table 1 lists the model names, main references, and CGILS contributors. It also gives the number of total vertical model layers and number of layers between the surface and 700 hPa in SCMs. The SCM vertical resolution in the boundary layer (PBL) is generally not sufficient to resolve the observed or LES simulated thin stratocumulus clouds. No attempt is made to make them finer since our objective is to understand the behavior of operational GCMs. For the LES models, however, because they are intended as benchmarks, much higher resolutions are used. The horizontal resolutions of LES models are 100 m, 50 m, and 25 m, respectively, at S6, S11, and S12. The vertical resolutions of the majority of LES are 40 m, 5 m, and 5 m, respectively, at the three locations. More detailed descriptions of the CGILS LES models are given in a companion paper by *Blossey et al.* [2013].

[16] The physical parameterizations in the SCMs relevant to the present study are the PBL, shallow convection, and cloud schemes. For PBL schemes, the generic form can be written in terms of turbulent flux at the model interfaces:

$$\overline{w'S'} = -K_c\left(\frac{\partial S}{\partial z} - \gamma_c\right), \qquad (3)$$

where z is height, w is vertical velocity, S is a conservative model prognostic variable. Prime represents the turbulent perturbation from the mean that is denoted by the overbar. K_c is the eddy diffusivity, and γ_c is the counter-gradient transport term. In addition to resolution, the differences in PBL schemes among the models are in their formulations of K_c and γ_c. For K_c, some models parameterize it by using local variables at the resolved scales, such as local Richardson number in the so-called first order closure models, or local turbulent eddy kinetic energy (TKE) [*Mellor and Yamada*, 1974]. Other models use nonlocal empirical parameterization of K_c as a function of height relative to the boundary layer depth. Another K_c difference among the models is its parameterization at the top of the PBL. While some models have explicit parameterizations of turbulent entrainment based on parameters such as cloud-top radiative and evaporative cooling, others do not consider entrainment. For the counter-gradient term γ_c, some models calculate it based on surface buoyancy fluxes, while others do not have this term. Table 2

Table 3. Shallow Convection Schemes[a]

Models Acronyms	References	Trigger	Lateral Entrainment	Lateral Detrainment	Closure
ACCESS	*Gregory and Rowntree* [1990] and *Grant* [2001]	Undiluted parcel	Specified	Specified	TKE
CAM4	*Hack* [1994]	Undiluted parcel	N	N	CAPE
CAM5	*Park and Bretherton* [2009]	CIN + TKE	Buoyancy sorting	Buoyancy sorting	CIN + TKE
CCC	*von Salzen et al.* [2012], *von Salzen and McFarlane* [2002], and *Grant* [2001]	Undiluted parcel	Buoyancy profile	Buoyancy profile	TKE
CLUBB	*Golaz et al.* [2002a, 2002], *Larson and Golaz* [2005], and *Golaz et al.* [2007]	N	N	N	High-order bi-normal distribution
ECHAM6	*Tiedtke* [1989]	Diluted parcel	Specified	Specified	Moisture con vergence
ECMWF	*Tiedtke* [1989]	Diluted parcel	Specified	Diagnosed	Subcloud moist static energy
EC-ETH	*Von Salzen and McFarlane* [2002], *Grant* [2001], and *Isotta et al.* [2011]	Undiluted	Buoyancy profile	Buoyancy profile	TKE
GFDL-AM3	*Bretherton and Park* [2009] and *Zhao et al.* [2009]	CIN + TKE	Buoyancy sorting	Buoyancy sorting	CIN + TKE
GISS	*Del Genio and Yao* [1993] and *Del Genio et al.* [2007]	Undiluted parcel	Buoyancy and speed	Above neutral level	Cloud-base buoyancy
GMAO	*Moorthi and Suarez* [1992]	Undiluted	Diagnosed	N	CAPE
HadGEM2	*Gregory and Rowntree* [1990] and *Grant* [2001]	Undiluted parcel	Specified	Specified	TKE
JMA	*Pan and Randall* [1998]	Diluted parcel	Diagnosed	N	Prognostic
IPSL	*Emanuel* [1991, 1993]	Undiluted parcel	Buoyancy sorting	Buoyancy sorting	CAPE
RACMO	*Neggers et al.* [2009a, 2009b]	Unified with PBL scheme	Unified with PBL scheme	Unified with PBL scheme	Unified with PBL scheme

[a]Some models use the same schemes for deep convections.

categorizes the PBL schemes in the SCMs according to the above attributes. Cloud-top entrainment in Table 2 refers to explicit parameterization. PBL schemes formulated using moist conserved variable and TKE closure (such as ECHAM6) may implicitly contain cloud-top entrainment. As can be seen, a wide variety of PBL parameterizations are used in the SCMs. Because of coarse vertical resolutions, however, some of these differences do not make as much of an impact on cloud simulations as they would if higher vertical resolutions were used.

[17] The majority of SCMs used mass-flux shallow convection schemes. The generic form of convective transport for a conservative variable q_t in these schemes is

$$\overline{w'q_t'} = M(z)(q_{tc} - q_{te}), \qquad (4)$$

where the prime denotes deviation of the bulk properties of clouds from the mean; M is the convective mass flux; subscripts c and e represent values in the parameterized cloud model and in the environment air, respectively. The convective mass flux is calculated from parameterized rates of entrainment and detrainment δ:

$$\frac{1}{M}\frac{\partial M}{\partial z} = \lambda - \delta.$$

[18] Some models do not separately parameterize shallow and deep convection. The schemes can differ in their entrainment and detrainment rates, the closure

that determines the amount of cloud base mass flux, and convection triggering condition as well as origination level of convection. Table 3 categorizes the convective schemes in the SCMs based on these main attributes. Among the SCMs, CLUBB, and RACMO use a single scheme to parameterize PBL turbulence and shallow convection.

[19] Cloud schemes in SCMs include a macrophysical and a microphysical component. Cloud macrophysical schemes parameterize cloud amount and the grid-scale rate of condensation and evaporation. These schemes can be generically described by assuming that the total water in the air, q_t, obeys a probability distribution function (pdf) $P(q_t)$ within a model grid box. The cloud amount is then

$$C = \int_{q_s}^{\infty} P(q_t) dq_t, \qquad (5)$$

where q_s is the saturation vapor pressure at cloud temperature. Cloud liquid water q_l is then

$$q_l = \int_{q_s}^{\infty} (q_t - q_s) P(q_t) dq_t. \qquad (6)$$

[20] Therefore, cloud fraction and cloud liquid water are often proportional to each other in individual models when the cloud fraction is less than 100%. The cloud microphysics scheme treats how condensed water is converted to precipitation. In most parameterizations,
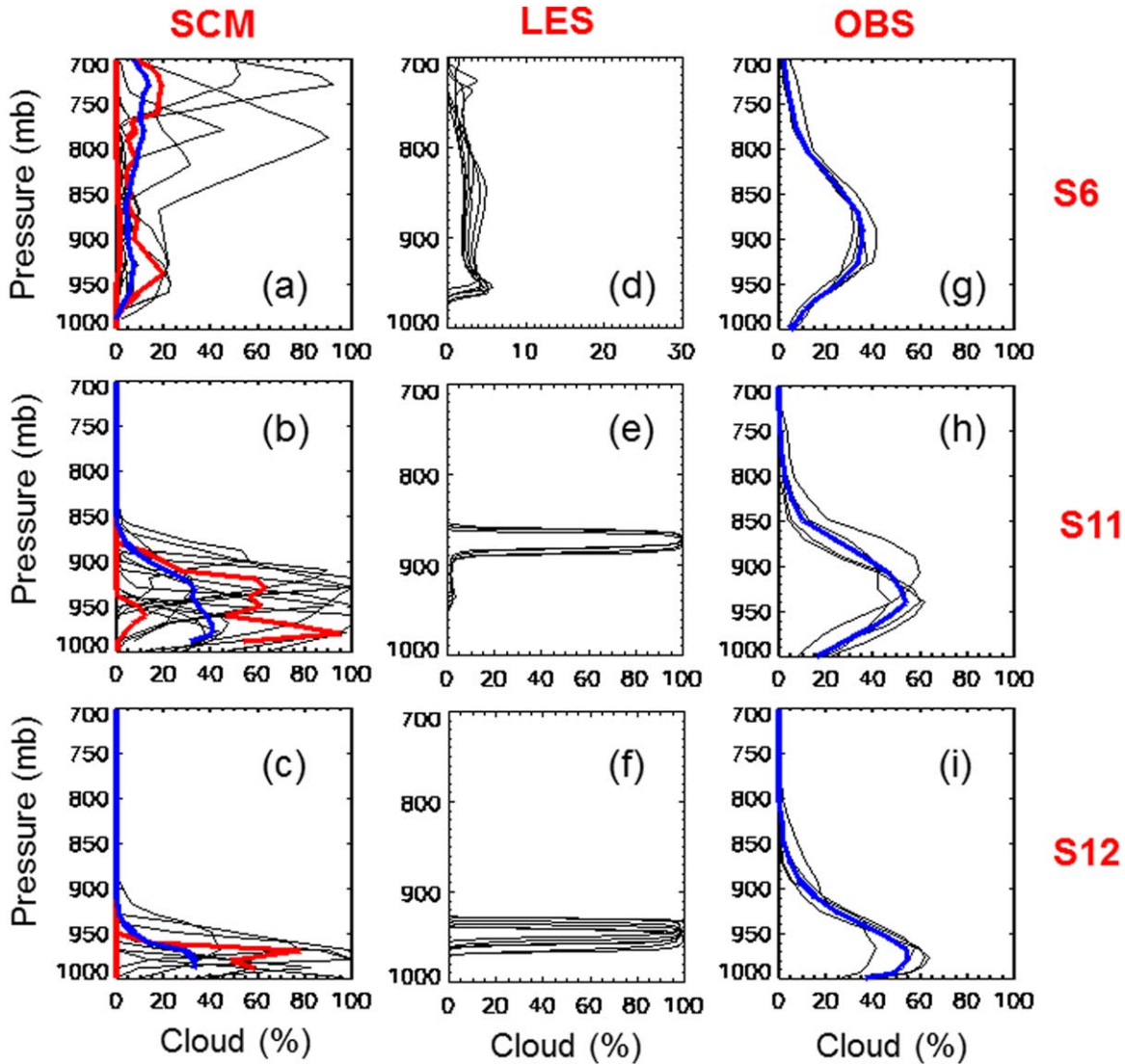
Figure 4. (a–c) Averaged profiles of cloud amount (%) by SCMs for S6, S11, and S12, respectively (from top to bottom plots). (d–f) Same as Figures 4a–4c but by the LES models. (g–i) From the C3M satellite measurements. The blue lines are ensemble averages; the red lines are the 25% and 75% percentiles.

precipitation is typically proportional to cloud water, which is further proportional to rate of large-scale condensation.

4. Simulated Clouds and Associated Physical Processes

[21] Before investigating cloud feedbacks, we first examine the simulated clouds in CTL. Figure 4 shows the time-averaged cloud profiles in all 15 SCMs and all LES models, with the shallow cumulus location S6 in the top row and the stratus location S12 in the bottom row. SCMs results are in the left column; LES models in the middle column; observations from C3M for the summers of 2006–2009 in the right column. Note that the observations may have categorized drizzle as clouds, therefore having a different definition of clouds from

that in the models. The blue lines denote the ensemble averages or multiyear averages; the red lines denote the 25 and 75 percentiles. Figure 5 shows examples of the time-pressure cross sections of these cloud amount from a sample of three SCMs (JAM, CAM4, and GISS), which are selected because they span the range of model differences as will be shown later, and from one LES (SAMA).

[22] Despite large differences among the models, the relative rank of cloud-top height and cloud amount at the three locations is correct. The spread in the LES models is much smaller than that among the SCMs. At S11, LES models simulated cumulus under stratocumulus. The use of the steady forcing for all models may have amplified the intermodel differences, since in both GCMs and the real atmosphere the large-scale circulation can respond to local differences in the inversion
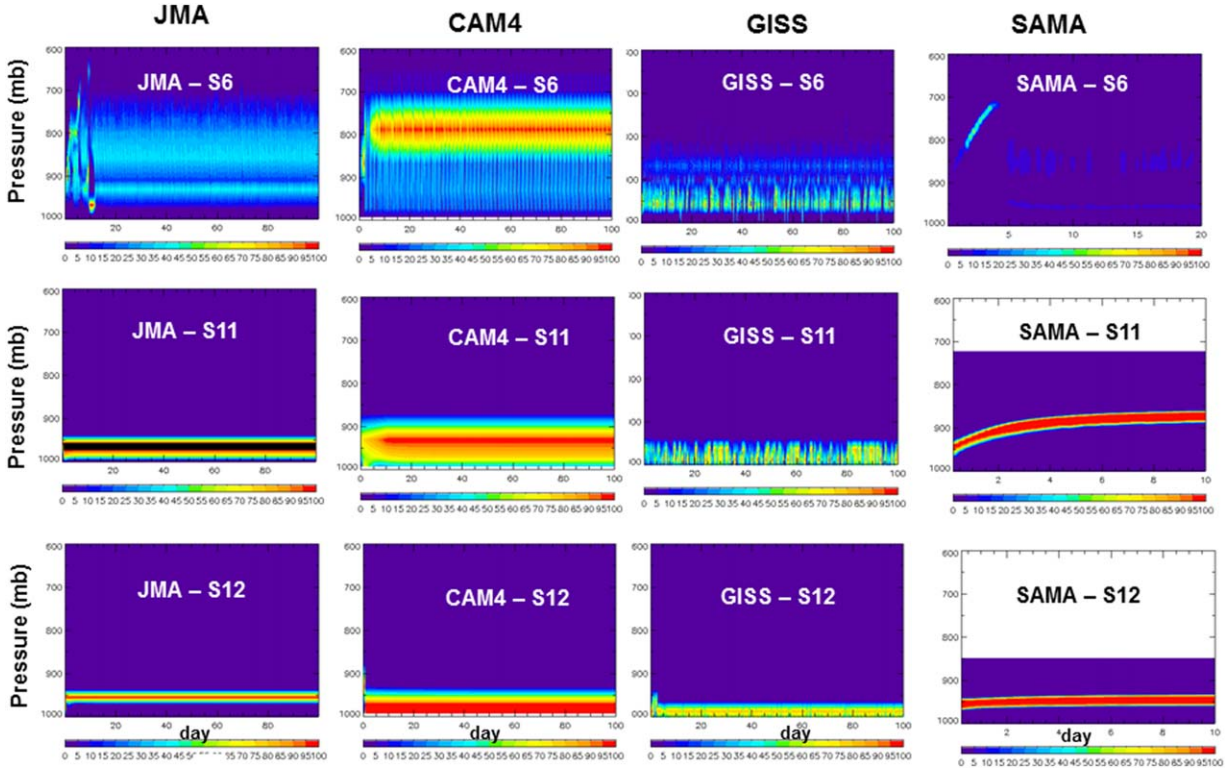
Figure 5. Examples of time evolution of cloud amount (%) simulated by JMA (left column) for S6, S11, and S12, respectively, from top to bottom plots; CAM4 (middle column); GISS (third column); SAMA (right column).

height by partially compensating them [*Blossey et al.*, 2009; *Bretherton et al.*, 2013].

[23] We find it instructive to use the following moisture budget equation to probe the physical parameterizations responsible for the simulated clouds in the SCMs. It is written as:

$$\frac{\partial q_v}{\partial t} = \left(\frac{\partial q_v}{\partial t}\right)_{turb} + \left(\frac{\partial q_v}{\partial t}\right)_{conv} - (c-e)_{stra} \\ - \left[\left(\vec{V}\cdot\nabla q\right)_{LS} + \omega_{LS}\frac{\partial q_v}{\partial p}\right], \tag{7}$$

where the variables are as commonly used, and the tendency terms have been separated into three physical terms representing parameterizations of PBL turbulence (*turb*), convection (*conv*), large-scale stratiform net condensation (*c-e*), plus the three-dimensional large-scale forcing. As will be shown later, the separation of the physical tendency terms helps to provide a framework of interpreting cloud feedback behaviors in the models. We show the three selected models in Figure 6 of the time-averaged profiles of these three terms at S11 in CTL by using the colored solid lines. The black lines are the simulated grid-box mean cloud liquid water. The solid dots on top of the black lines donate the midpoint of model layer.

[24] In the JMA model, only two physical terms are active (Figure 6a) in addition to the large-scale dynamic forcing. The PBL scheme moistens the boundary layer; the large-scale condensation dries it. The residual is balanced by the drying from the large-scale forcing. The peak altitudes of the "*turb*" and "*c-e*" are the same as that of the cloud liquid water. Since the PBL scheme is always active, the stratiform condensation scheme responds to the PBL scheme. In CAM4, Figure 6b shows that shallow convection is active in addition to the "*turb*" and the "*c-e*" terms. The shallow convective scheme transports the moisture from the boundary layer to the free troposphere. In the GISS model, Figure 6c shows that shallow convection is also active, but unlike CAM4, the maximum drying of the "*conv*" term is at the same level as the maximum level of "*turb*," in the middle of the cloud layer. These differences will be shown later as causes of different cloud feedbacks in the models. In Figure 6, the stratiform condensation term is the direct source of cloud water.

[25] The intermodel differences in Figure 6 are examples of how different parameterization assumptions can affect the balance of the physical processes and associated clouds. The JMA model used the prognostic Arakawa-Schubert convection scheme [*Pan and Randall*, 1998] with fixed cloud base level near 900 hPa in the model [*JMA*, 2013]. As a result, convection is not active in this case. CAM4 and GISS both used positive Convective Available Potential Energy (CAPE) of undiluted air parcels as criteria of convection. As a result, shallow convection is more easily triggered in these two
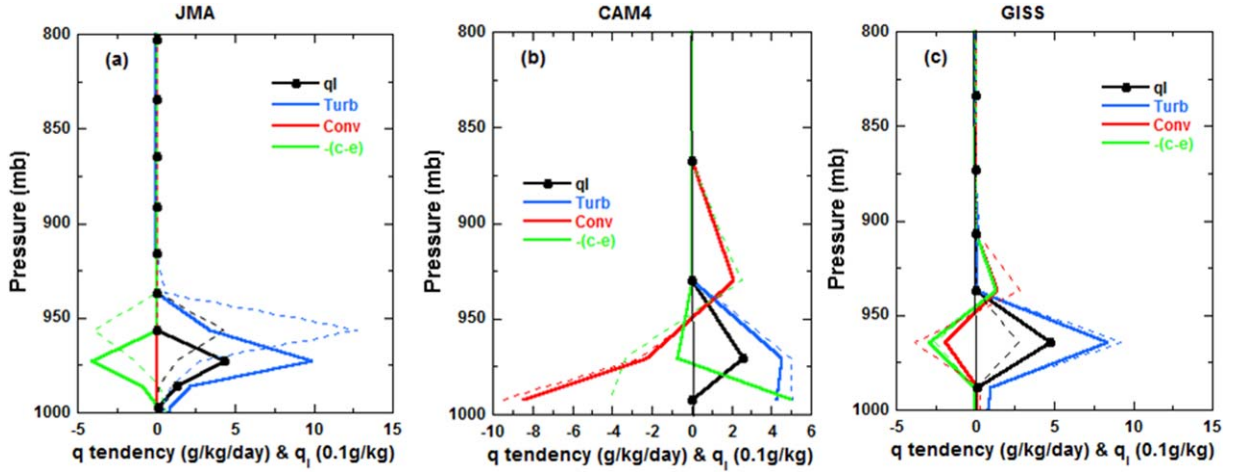
Figure 6. Solid lines are physical tendencies of water vapor (g/kg/day) in three SCMs at S11 for the control climate, "*turb*" for turbulence scheme, "*conv*" for convection scheme, "*(c-e)*" for net large-scale condensation, and "*ql*" for the grid-box cloud liquid water (0.1 g/kg). The black dots show the midpoint of model layers. The dashed lines show the corresponding values in the warmer climate. (a) JMA, (b) CAM4, and (c) GISS.

models. Nevertheless, the assumptions in their shallow convection parameterizations are different. For example, CAM4 does not include lateral entrainment into the convective plumes [*Hack*, 1994], while GISS has lateral entrainment [*Del Genio and Yao*, 1993].

[26] Tables 4–6 show the simulated surface sensible and latent fluxes, precipitation, cloud water path, and cloud-radiative effects in the SCMs at S12, S11, and S6, respectively, in the control climate. Total cloud amount is not included in the table since in some models it is contaminated by unrealistic optically thin clouds in the upper troposphere. The expected increase of surface latent heat fluxes from S12 to S11 and S6 is simulated in most models. However, consistent with what has been shown in the vertical profiles of clouds in Figure 4,

the models differ greatly in their cloud liquid water path, and as a result, in the shortwave cloud radiation effect. At S12, some models did not simulate clouds. As shown in *Zhang et al.* [2012] for the GFDL model, this unrealistic behavior is related to the use of steady forcing. When compared with the LES results of Tables 3–5 in *Blossey et al.* [2013], the SCM surface latent heat fluxes are generally smaller than in the LES models. This is likely related to the use of the steady forcing or insufficient entrainment mixing in the SCMs. The precipitations and the cloud liquid paths in the SCMs span a wide range that brackets the corresponding range in the LES models. Since the objective of CGILS is to investigate the cloud feedback or the response of the cloud fields to a warmer climate, we only use Figure 6

Table 4. Simulated Fields in Control Climate and Their Changes in the Perturbed at S12 in SCMs[a]

Model_ID	SH	LH	PREC	TGLWP	SWCRF	CRE
ACCESS	13.8 (−5.8)	58.9 (−2.8)	0.00 (0.00)	14.2 (−5.4)	−79.4 (35.4)	−72.2 (32.3)
CAM4	24.7 (−0.6)	48.3 (4.6)	0.00 (0.00)	199.4 (11.0)	−210.4 (−0.6)	−215.5 (−1.0)
CAMS	−6.0 (0.2)	2.9 (0.3)	0.00 (0.00)	0.0 (0.0)	0.0 (0.0)	0.0 (0.0)
CCC	26.6 (−3.6)	54.4 (13.1)	0.51 (−0.14)	186.2 (−82.5)	−100.4 (17.2)	−100.3 (19.5)
CLUBB	25.8 (−1.6)	64.7 (11.4)	0.00 (−0.00)	77.8 (24.2)	−176.2 (−18.2)	−170.5 (−18.0)
ECHAM6	−22.8 (1.9)	62.2 (2.9)	1.10 (0.10)	98.1 (0.9)	−121.4 (0.8)	−124.1 (1.6)
ECMWF	10.1 (−3.7)	68.1 (15.4)	0.00 (−0.00)	12.5 (3.8)	9.9 (−5.4)	12.8 (−4.2)
EC_ETH*	−27.9 (43.7)	1.5 (32.8)	0.00 (0.0)	0.0 (0.0)	0.0 (0.0)	0.0 (0.0)
GFDL_AM3	−4.8 (1.1)	18.9 (2.6)	0.00 (0.00)	0.0 (0.0)	0.0 (0.0)	0.0 (0.0)
GISS	11.3 (−0.5)	59.9 (10.7)	0.35 (0.22)	140.9 (95.1)	−109.0 (−24.5)	−108.2 (−24.3)
GMAO	1.3 (0.2)	35.5 (2.1)	0.50 (−0.50)	0.8 (−0.8)	−1.0 (0.9)	−1.3 (1.2)
HadGEM2	17.0 (−1.8)	61.2 (7.2)	0.70 (−0.30)	23.9 (−4.4)	−95.5 (13.5)	−88.7 (13.4)
IPSL	25.0 (−1.6)	66.4 (5.4)	0.72 (0.80)	47.1 (0.3)	−65.1 (0.0)	−66.4 (0.5)
JMA	27.0 (−0.4)	62.3 (4.9)	0.31 (0.70)	48.7 (7.2)	−122.8 (−8.4)	−122.4 (−8.5)
RACMO	20.2 (−3.5)	68.2 (11.9)	0.40 (−0.20)	34.3 (8.l)	−33.4 (−6.2)	−27.6 (−6.2)

[a]Numbers in the parentheses are the changes in the perturbed climate. Listed are sensible and latent heat fluxes (SH, LH, in W/m²), precipitation (PREC, mm/day), total cloud water path (TGLWP, g/m²), shortwave, and total cloud-radiative effect (SWCRE, CRE, W/m²). The asterisk denotes that the model has not reached equilibrium state (the EC_ETH model).

Table 5. Same as Table 4 but for S11

Model_ID	SH	LH	PREC	TGLWP	SWCRE	CRE
ACCESS	11.9 (−1.8)	84.1 (7.4)	0.26 (0.50)	65.0 (−10.8)	−123.0 (29.1)	−113.9 (26.4)
CAM4	23.7 (0.4)	59.3 (7.9)	0.00 (0.00)	77.2 (4.8)	−133.4 (−1.7)	−129.7 (−1.4)
CAM5	15.1 (−0.3)	90.2 (9.1)	0.00 (0.20)	55.0 (14.9)	−124.1 (2.3)	−116.4 (2.8)
CCC	29.7 (−4.4)	63.3 (22.8)	0.70 (−0.33)	228.2 (−76.8)	−107.2 (14.8)	−100.8 (17.4)
CLUBB	4.2 (0.7)	88.5 (8.2)	0.00' (0.00)	25.3 (6.3)	−95.7 (−14.7)	−78.5 (−13.6)
ECHAM6	−21.4 (1.7)	78.4 (5.6)	1.33 (0.90)	173.1 (3.0)	−150.8 (0.4)	−150.9 (0.7)
ECMWF	6.8 (−0.6)	87.2 (12.3)	0.80 (0.13)	48.7 (15.1)	−24.6 (−7.2)	−17.3 (−6.3)
EC_ETH	6.5 (5.3)	73.1 (15.4)	0.31 (0.39)	144.4 (35.0)	−129.4 (−7.1)	−130.1 (−3.5)
GFDL_AM3	15.5 (−6.3)	78.7 (15.8)	0.30 (0.50)	40.0 (5.5)	−118.4 (−11.8)	−111.3 (−11.2)
GISS	10.8 (0.5)	76.3 (5.4)	0.43 (−0.07)	129.8 (−55.7)	−68.1 (25.8)	−66.2 (25.1)
GMAO	5.1 (−0.1)	84.9 (8.0)	0.70 (0.11)	10.0 (10.7)	−11.8 (−9.8)	−10.2 (−8.2)
HadGEM2	7.4 (−0.2)	69.7 (5.3)	0.00 (−0.00)	4.7 (−3.3)	−27.3 (9.4)	−24.5 (8.7)
IPSL	23.5 (−0.9)	74.7 (7.6)	0.76 (0.11)	52.2 (-O.0)	−69.3 (0.4)	−63.5 (0.7)
JMA	26.9 (−4.1)	73.1 (14.5)	0.59 (0.50)	80.3 (20.1)	−157.1 (−13.9)	−151.5 (−15.4)
RACMO	15.3 (−2.3)	91.0 (8.9)	0.24 (−0.18)	100.9 (−5.5)	−85.7 (4.5)	−74.7 (4.8)

as an illustration of why the SCMs simulated different clouds in the control climate.

5. Cloud Feedbacks

5.1. SCM Results at S11 (Stratocumulus)

[27] We first use the cumulus under stratocumulus regime S11 to establish a framework to interpret the cloud feedbacks in the 15 SCMs. Figure 7 shows the change of net CRE from CTL to P2S at S11. Increase of CRE in the figure means positive cloud feedbacks; decrease of CRE means negative feedbacks. For simplicity, the change of CRE is referred to as cloud feedback. The 15 SCMs simulated negative and positive cloud feedbacks that span a rather wide range of about 40 W/m². *Blossey et al.* [2013] showed this range as about 10 W/m² in LES models. Because of the simplified CGILS setup, we do not expect the feedbacks here to be the same as in the full GCMs, but they allow us to gain some insight into the physical processes that determine them.

[28] In Figure 7, the character "X" above a model's name indicates that shallow convection is not triggered in both the CTL and P2S simulations of this model. The character "O" above a model's name indicates that shallow convection is active in at least one of the simulations of CTL and P2S. PBL schemes are always trig-

gered in all models. Models without these characters about their names used unified schemes of turbulence and shallow convection (such as CLUBB and RACMO) or did not submit information for convection (such as ECMWF). One can see that models without active shallow convection tend to simulate negative cloud feedbacks, while models with active convection tend to simulate positive cloud feedbacks.

[29] Without convection, as discussed in the previous section for the JMA model, the water vapor balance is achieved by a competition between the moistening effect of the "*turb*" term in equation (7) and drying effect of the net large-scale condensation "*c-e*" term and large-scale forcing; clouds are caused by the moistening term from the PBL scheme. Therefore, the response of the PBL scheme to SST largely determines the change of cloud water, hence, the cloud feedbacks. Even though cloud microphysical and precipitation processes can also influence cloud feedbacks, as mentioned before, since precipitation is typically proportional to cloud water, cloud water controls the net change of condensates in the simulations.

[30] The PBL moistening term at the altitude of maximum cloud liquid water is larger in the warmer climate in virtually all models as shown in Figure 8a. In the one exception of the CCC model, the simulated altitude of

Table 6. Same as Table 4 but for S6

| Model_ID	SH	LH	PREC	TGLWP	SWCRE	CRE
ACCESS	6.8 (−0.4)	111.4 (10.9)	1.02 (0.16)	19.8 (0.9)	−9.6 (−0.4)	−9.0 (−0.4)
CAM4	8.5 (0.0)	105.3 (12.2)	0.00 (0.00)	247.9 (24.0)	−177.4 (−4.5)	−161.0 (−5.6)
CAM5	6.5 (−0.2)	104.3 (13.4)	0.74 (0.16)	24.3 (−3.4)	−35.2 (8.2)	−34.2 (8.1)
CCC	9.0 (0.5)	122.4 (7.3)	1.59 (0.60)	68.9 (−34.2)	−35.4 (24.9)	−27.3 (18.7)
CLUBB	10.4 (−0.1)	119.5 (10.2)	0.57 (−0.10)	31.8 (−0.6)	−91.7 (1.4)	−73.7 (−0.1)
ECHAM6	−5.6 (−0.7)	102.5 (9.2)	0.79 (0.00)	183.2 (8.2)	−181.6 (−0.1)	−146.6 (−4.1)
ECMWF	7.9 (0.6)	108.1 (8.5)	0.86 (0.70)	25.5 (6.0)	−12.6 (−2.5)	−7.1 (−2.5)
EC_ETH	2.8 (−1.2)	104.8 (7.6)	0.61 (0.10)	130.0 (5.0)	−125.5 (2.8)	0.0 (0.0)
GFDL_AM3	8.8 (−0.6)	110 (9.3)	0.84 (0.12)	5.9 (1.1)	−12.7 (−13.3)	−11.7 (−13.4)
GISS	11.4 (−0.9)	125.6 (10.0)	1.41 (0.11)	18.8 (−4.2)	−41.9 (12.8)	−39.4 (11.4)
GMAO	6.1 (−1.9)	116.5 (6.1)	1.14 (0.11)	59.0 (1.3)	−37.4 (1.0)	−33.1 (0.8)
HadGEM2	6.0 (−0.4)	109.9 (9.9)	0.98 (0.12)	3.7 (0.7)	−22.0 (−0.9)	−20.1 (−1.1)
IPSL	10.2 (−0.5)	118.8 (10.7)	1.34 (0.17)	74.6 (−1.6)	−59.0 (4.7)	−53.6 (4.0)
JMA	14.7 (−0.1)	108.2 (7.8)	0.63 (0.70)	179.8 (25.3)	−107.0 (−5.9)	−101.2 (−6.3)
RACMO	12.0 (−0.5)	108.2 (8.1)	0.66 (0.60)	63.2 (7.6)	−28.4 (−1.6)	−25.8 (−1.7)
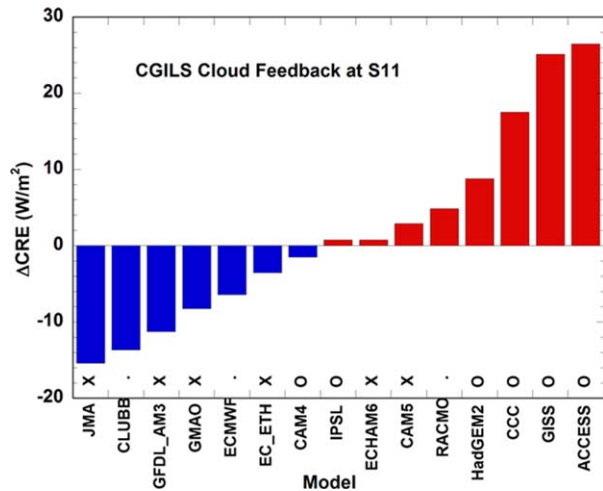
Figure 7. (a) Change of cloud-radiative effect (CRE, W/m^2) in SCMs at location S11 corresponding to 2 K SST perturbation. Character "X" above a model's name indicates that the shallow convection scheme is not active; "O" indicates that the shallow convection scheme is active. Models without these characters either do not separately parameterize shallow convection and PBL turbulence, or do not submit results with convection information.

maximum cloud water in P2S is much higher than in CTL, above the top of the boundary layer (not shown), where the turbulent term is small. The increased moistening by the PBL schemes is generally consistent with the increase of surface latent heat flux (LHF) in P2S, as shown in Figure 8b. The increase of latent heat flux with SST is consistent with CGILS LES simulations in *Blossey et al.* [2013] (their Table 4) and in earlier LES studies under similar experimental setup [e.g., *Xu et al.*, 2010]. Also, *Liepert and Previdi* [2012] showed that in virtually all 21st century climate change simulations by CMIP3 models, surface latent heat fluxes are larger in a warmer climate over the oceans (their Table 2, column 3).

[31] Previous studies [e.g., *Caldwell and Bretherton*, 2009] have shown negative cloud feedbacks in mixed layer models (MLM) and have attributed the mechanism to larger surface latent heat flux and weaker large-scale subsidence in a warmer climate. These two conditions are also shown in the CGILS SCM models that do not trigger convection. Table 5 shows that cloud water path in the negative feedback models is increased in the warmer climate. The example in Figure 6a (dashed lines) for the JMA model also illustrates the larger moistening rate by turbulence and deeper cloud layer in the warmer climate. The CGILS results are therefore consistent with the interpretation of the negative feedbacks in MLMs. Exceptions are noted in which the convective scheme is not active in a model, but the model has small positive cloud feedbacks, such as in CAM5 and ECHAM6. These may be related with cloud-top entrainment, included explicitly and implicitly in these models, which acts like shallow convection.

Taking the ensemble of models as a whole, we can use Figure 9a to schematically summarize the negative cloud feedbacks in the SCMs without convection. In these models, accompanied by the weaker large-scale subsidence, the warmer climate has greater surface latent heat flux, larger turbulence moisture convergence in the cloud layer, and consequently an inclination to give the negative cloud feedbacks. This mechanism is not new, but we see that it can explain the SCM results in CGILS without activated convection.

[32] We now turn to models with active shallow convection. Figure 7 shows that these models tend to have positive cloud feedbacks. As discussed in the previous section for CAM4 and GISS, shallow convection acts to dry the cloud layer. It is a moisture sink that has the same sign as the stratiform condensation sink in equation (7). The enhanced moistening from the PBL scheme in the warmer climate is approximately balanced by enhanced drying from the sum of the stratiform condensation and shallow convection. If the rate of drying from the shallow convection is greater than the rate of moistening from the PBL scheme as SST increases, the stratiform condensation can decrease in a warmer climate. This tends to reduce cloud water and clouds, thus causing positive cloud feedback. The enhanced rate of convective drying in the warmer climate may be explained by the moisture flux in equation (4) immediately above the top of the boundary layer. The moisture contrast is larger in the warmer climate, since the subsiding free tropospheric air remains dry but the total water in convective plumes increases with SST. An example is shown in Figure 6c for the GISS
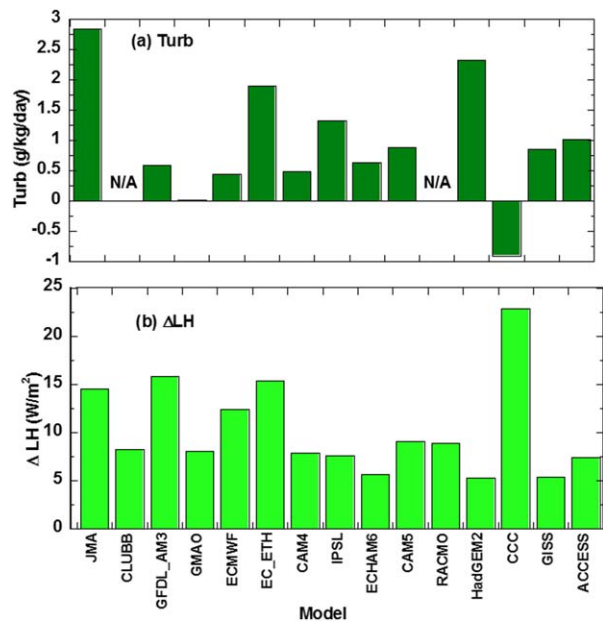

Figure 8. (a) Change of moisture tendency in the layer of maximum cloud water (g/kg/day) by the "*Turb*" term from the control climate to the perturbed climate at S11. (b) Same as Figure 8a but for surface latent heat flux (W/m^2).
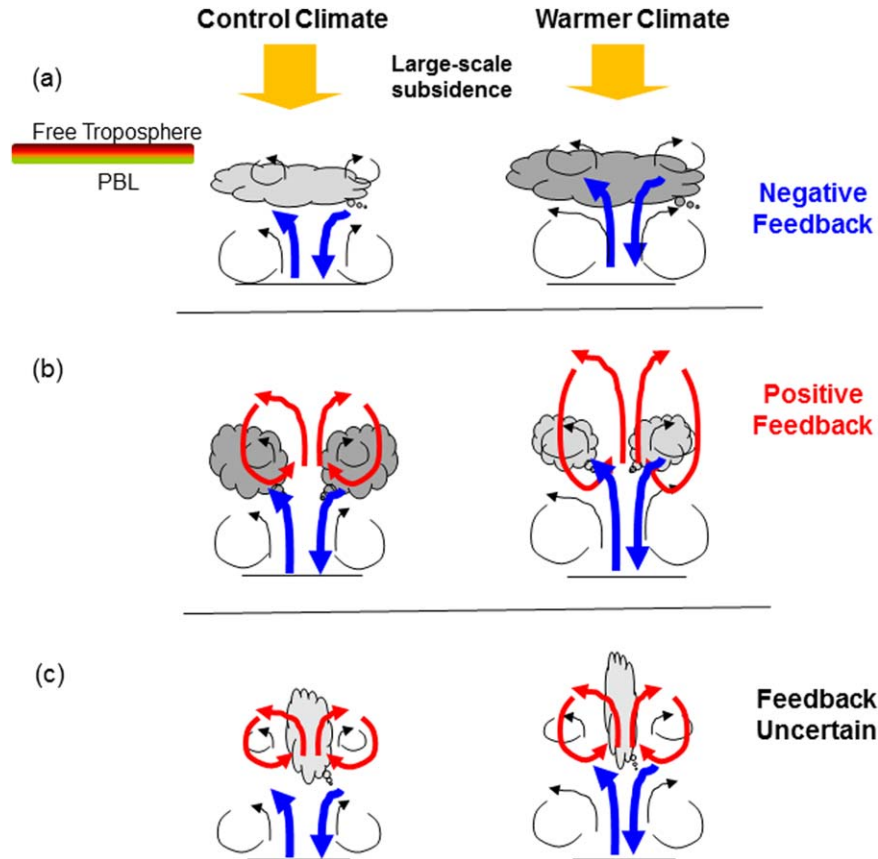
Figure 9. Schematics of cloud feedbacks. Changes of clouds from the (left) control to (right) warmer climates. Blue arrows denote the term of turbulence parameterization in the moisture budget equation; red arrows denote shallow convection. The sizes of arrows schematically correspond to the magnitude of moisture tendency from the associated processes. (a) Negative cloud feedback, dominated by the increase of surface turbulence, the "NESTS" negative cloud feedback mechanism (see text). (b) Positive cloud feedback, dominated by the increase of shallow convection or cloud-top entrainment, the "SCOPE" positive cloud feedback mechanism (see text). (c) Cloud feedback from shallow cumulus of sufficient depth, with sign depending on cloud depth and lateral mixing.

model by using the dashed lines. In the warmer climate, there is increase of turbulence moistening, but larger increase of convective drying, and therefore reduced cloud water. Active convection therefore causes larger ventilation of the cloud layer in a warmer climate, which tends to decrease clouds and cause positive cloud feedbacks. This increase of convective mixing of boundary layer air together with the change of cloud-top entrainment causes more dilution of the cloudy layer and therefore positive feedback. We can therefore use Figure 9b to schematically summarize the positive cloud feedbacks in the models. The net cloud feedbacks can be considered as due to two opposing roles of surface-based PBL turbulence and shallow convection aided by cloud-top entrainment, with the latter dominating in most of the models in which convection is active. Figure 9b also applies to models with parameterizations of significant cloud-top entrainment. The PBL scheme can also be dominant over the shallow convection scheme in some models, such as in CAM4. In this model, as discussed in the previous section, the peak drying of shallow convection occurs below the cloud layer instead of within the cloud layer.

[33] *Brient and Bony* [2012] used the larger moisture contrast between the free troposphere and boundary layer in the warmer climate to explain the positive cloud feedbacks in the IPSL SCM and GCM, while *Kawai* [2012] used the increased surface flux to explain the negative cloud feedback in the JMA SCM and GCM. These are consistent with the present interpretation. Figure 7 shows that in CGILS when convection is active, the positive feedback dominates the negative feedback. In GCMs or in the real atmospheres, any changes in the frequency of convection and convective mass fluxes would also matter. We call the above two competing mechanisms in Figure 9 as the "NESTS-SCOPE" (Negative feedback from Surface Turbulence under weaker Subsidence—Shallow Convection PositivE feedback) mechanisms. Obviously, given the wide range of physical parameterizations in models, this interpretation may not fit all models. For example, *Zhang and Bretherton* [2008] showed that in CAM3 the interaction of an unintended deep convection with the cloud microphysical scheme caused a negative cloud feedback in that model. Nevertheless, the delineation of the two
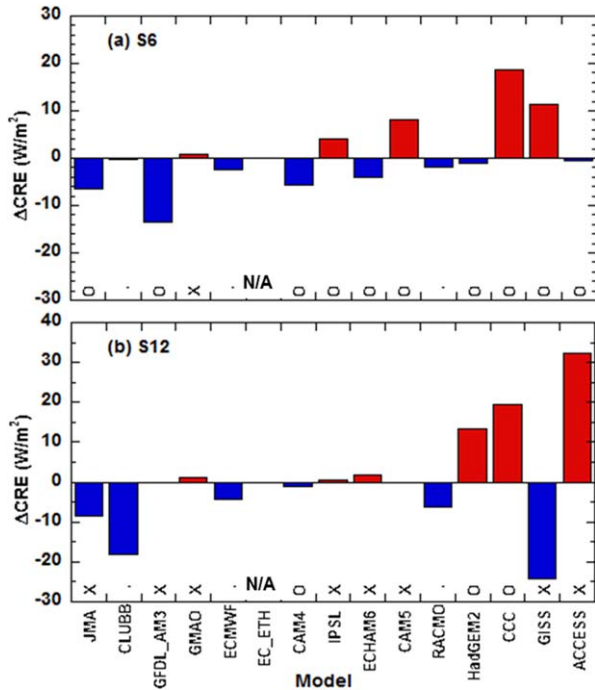
Figure 10. Same as Figure 7, but for (a) S6, (b) S12. The models are ordered in the same sequence as in Figure 7. One model (EC_ECH) did not reach quasi-equilibrium state and it is indicated by "N/A".

competing mechanisms is a useful framework to interpret the majority of models.

5.2. SCM Results at S6 (Shallow Cumulus) and at S12 (Coastal Stratus)

[34] We now use the same framework as we used for S11 to interpret SCMs results at the other two locations. Before proceeding, we need to supplement our schematics with another scenario in which the depth of convection is large and mixing of cloudy air with dry air can occur laterally. If the cloud-scale dynamical fields and the environmental relative humidity are the same, larger drying from convection is expected in P2S than CTL because of the larger difference of the absolute humidity of moisture across cloud lateral boundaries just like across cloud tops. This is schematically shown in Figure 9c. Other factors such as cloud-scale dynamics, cloud depth, and cloud microphysics can also change in a warmer climate, leading to more complicated behavior of cloud feedbacks for thicker clouds. This scenario also includes regime change of clouds from stratocumulus to shallow cumulus as exhibited by some models (e.g., CCC at S11, not shown).

[35] Figure 10a shows the SCM cloud feedbacks at the shallow convection location S6, with a range of about 30 W/m^2 (in LES, models, the range is less than 3 W/m^2). The models are ordered in the same sequence as in Figure 7. Almost all models simulated convection at S6. Cloud feedbacks are generally consistent with the change of cloud liquid water path (Table 6). Partially

due to the complications described above, convection at S6 does not necessarily correspond to positive cloud feedbacks. In all simulations, surface latent heat flux is greater in the warmer climate (Table 6). We may therefore use the same framework as for S11 to think that the larger surface latent heat flux alone is a factor for more clouds in a warmer climate, but the other factors from shallow convection such as lateral mixing favor more dilution of clouds and a positive cloud feedback. The two effects compensate each other differently in the models because of the different assumptions in the specific parameterizations.

[36] Figure 10b shows SCM results at S12, where SST is colder and subsidence is stronger than at S11. The corresponding changes of surface turbulent fluxes and cloud water path are given in Table 5. Clouds are restricted to within the boundary layer. The simulated cloud feedbacks also span a wide range. Three models simulated no clouds at this location (GFDL AM3, EC-ETH, and CAM5) (due to the constancy of forcing). Most models simulated the same cloud feedback signs as at S11. Some simulated opposite signs, one of which is the GISS model. As indicated by the "X" character above the GISS model in Figure 10b, for this model, shallow convection is not active at S12, in contrast to be active at S11. Consistent with our hypothesis, the cloud feedback changed from positive to negative. The conceptual framework in Figures 9a and 9b can be generally applied to describe the behavior of cloud feedbacks in the SCMs at S12.

5.3. LES Results

[37] The CGILS LES results have been summarized in *Blossey et al.* [2013]. To compare with SCM results, in Figures 11a–11c, we show the LES cloud feedbacks at the three locations of S6, S11, and S12, respectively. The LES results are more consistent with each other than SCMs. At the shallow cumulus location S6 (Figure 11a), LES models simulated a small positive cloud feedback except for DALES and WRF that had negligible feedbacks. At the stratocumulus location S11 (Figure 11b), all models except for SAM simulated positive cloud feedbacks. At the coastal stratus location S12 (Figure 11c), all except for DALES simulated negative cloud feedback. There is therefore consensus, but not uniform agreement, among the LES models with regard to simulated cloud feedbacks.

[38] *Blossey et al.* [2013] attributed the negative feedback at S12 to the deepening of the cloud layer in a relatively well-mixed boundary layer that is related to weaker large-scale subsidence in the warmer climate. As mentioned before, this is also the interpretation of MLM negative cloud feedback and in the SCMs of CGILS as shown in Figure 6a. In some SCMs, vertical resolutions are not sufficient, so the deepening of clouds cannot be simulated. In these models, the weaker subsidence leads to less subsidence drying in the warmer climate. This is accompanied by larger turbulent convergence of moisture into the cloud layer from enhanced surface flux and more liquid water. Therefore, the SCM interpretations are still consistent with the
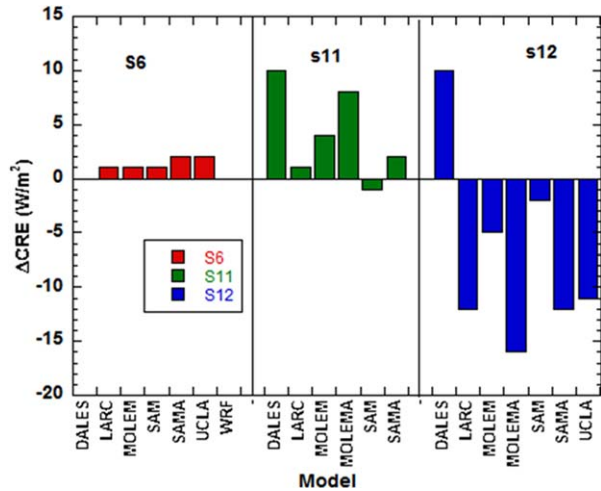
Figure 11. Same as Figure 7 but in LES models. (a) S6, (b) S11, and (c) S12.

LES results of deepening boundary layer. At S11, *Blossey et al.* [2013] attributed the positive feedback in the LES models to cloud thinning in a warmer climate caused by decoupling of the boundary layer with the stratocumulus layer. In SCMs, the decoupled mixing is calculated by either shallow convection or cloud-top entrainment or both, which has been shown to cause positive cloud feedbacks as in Figure 6c. At S6, *Blossey et al.* [2013] attributed the positive feedback to more precipitation.

[39] A companion paper by *Bretherton et al.* [2013] investigated the sensitivity of LES results to large-scale conditions, including separate changes in surface forcing, large-scale subsidence, environmental relative humidity, and CO_2 concentration. These are not studied here since in CGILS we only aim at the total derivate of cloud feedback to imposed SST forcing with implied change in large-scale subsidence. The potential impact of the change of CO_2 forcing is left for future study. We point out that the consensus among the LES models in Figure 11 does not necessarily mean they simulated the correct cloud feedbacks. Nevertheless, they give plausible answers for SCMs to target for. Eventually, they need to be validated by observations under more realistic experimental setups.

6. Summary and Discussion

[40] The experimental setup of CGILS was used to simulate shallow cumulus, stratocumulus, and coastal stratus and to investigate the physical mechanisms of cloud feedbacks under idealized climate change in single column models. In models where shallow convection is not activated or plays minor role in drying the cloud layer, cloud feedbacks tend to be negative. In models when convection is active, cloud feedbacks tend to be positive in the stratocumulus and coastal stratus regime, but uncertain in the shallow cumulus regime. A framework is described to interpret the SCM cloud feedbacks by using the two opposing effects of increased moisten-

ing from PBL scheme under weaker large-scale subsidence and enhanced drying from shallow convection in a warmer climate, with the former causing negative cloud feedbacks and the convective scheme causing positive cloud feedbacks. The convective scheme plays a more dominant role at times when it is active. These mechanisms are summarized as the NESTS negative feedback and SCOPE positive feedback mechanisms. LES models simulated overall consistent positive cloud feedbacks in the shallow cumulus and stratocumulus regimes, but negative feedbacks in the coastal stratus regime. The LES results tend to support the NESTS-SCOPE mechanisms.

[41] The relevance of CGILS results to cloud feedbacks in GCMs and in real-world climate changes is not clear yet. In a preliminary comparison to cloud feedbacks in four GCMs at the three locations, SCMs results were uncorrelated to those simulated by the parent GCM, suggesting the complexity of translating the results from SCMs to the feedbacks simulated by GCMs. While CGILS is motivated by understanding the physical mechanisms of cloud feedbacks in GCMs, there are several issues that limit the applicability of the SCM results. First, the idealized forcing is steady state. Diurnal and synoptic variabilities are not considered. Second, the large-scale fields are not interactive with clouds. Third, the spatial variability of GCM cloud feedback may be large and so direct comparison at the selected locations may be inappropriate. Furthermore, the pattern of atmospheric large-scale condition in the GCMs may shift locations in a warmer climate [*Webb and Lock*, 2012]. Future phases of CGILS will investigate how results from the simplified case study should be used or how the case study should be modified to better understand cloud feedbacks in more complex models and in observations. The CGILS results highlight the desirability to treat physical parameterizations in General Circulation Models (GCMs) as an integrated system rather than individual components in order to reduce cloud feedback uncertainties.

References

Andrews, T., J. M. Gregory, M. J. Webb, and K. E. Taylor (2012), Forcing, feedbacks and climate sensitivity in CMIP5 coupled atmosphere-ocean climate models, *Geophys. Res. Lett.*, *39*, L09712, doi:10.1029/2012GL051607.

Blossey, P. N., C. S. Bretherton, M. Zhang, A. Cheng, S. Endo, T. Heus, Y. Liu, A. Lock, S. R. de Roode, and K.-M. Xu (2013), Marine low cloud sensitivity to an idealized climate change: The CGILS LES Intercomparison, *J. Adv. Model. Earth Syst.*, *5*, 234–258, doi:10.1002/jame.20025.

Blossey, P. N., C. S. Bretherton, and M. C. Wyant (2009), Understanding subtropical low cloud response to a warmer climate in a super-parameterized climate model. Part II: Column modeling with a cloud-resolving model, *J. Adv. Model. Earth Syst.*, *1*, 8, 14 pp., doi:10.3894/JAMES.2009.1.8.

Bretherton, C. S., and S. Park (2009), A new moist turbulence parameterization in the community atmosphere model, *J. Clim.*, *22*, 3422–3448, doi:10.1175/2008JCLI2556.1.

Bretherton, C. S., P. N. Blossey, and C. R. Jones (2013), A large-eddy simulation of mechanisms of boundary layer cloud response to climate change in CGILS, *J. Adv. Model. Earth Syst.*, doi:10.1002/jame.20019, in press.

Brinkop, S., and E. Roeckner (1995), Sensitivity of a general circulation model to parameterizations of cloud–turbulence interactions in the atmospheric boundary layer, *Tellus, Ser. A*, *47*, 197–220.

Bony, S., and J.-L. Dufresne (2005), Marine boundary layer clouds at the heart of cloud feedback uncertainties in climate models, *Geophys. Res. Lett.*, *32*, L20806, doi:10.1029/2005GL023851.

Bony, S., and K. A. Emanuel (2005), On the role of moist processes in tropical intraseasonal variability: Cloud–radiation and moisture–convection feedbacks, *J. Atmos. Sci.*, *62*, 2770–2789, doi:10.1175/JAS3506.1.

Bony, S., et al. (2006), How well do we understand climate change feedback processes? *J. Clim.*, *19*, 3445–3482.

Brient, F., and S. Bony (2012), Interpretation of the positive low cloud feedback predicted by a climate model under global warming, *Clim. Dyn.*, *6*, 1–17, doi:10.1007/s00382-011-1279-7.

Caldwell, P., and C. S. Bretherton (2009), Response of a subtropical stratocumulus-capped mixed layer to climate and aerosol changes, *J. Clim.*, *22*, 20–38.

Cess, R. D., et al. (1990), Intercomparison and interpretation of cloud-climate feedback processes in nineteen atmospheric general circulation models, *J. Geophys. Res.*, *95*, 16,601–16,615.

Dee, D. P., et al. (2011), The ERA-Interim reanalysis: Configuration and performance of the data assimilation system, *Q. J. R. Meteorol. Soc.*, *137*, 553–597, doi:10.1002/qj.828.

Del Genio, A. D., and M. Yao (1993), Efficient cumulus parameterization for long-term climate studies: The GISS scheme, in *The Representation of Cumulus Convection in Numerical Models,* vol. *46,* Meteorological Monographs, edited by K. A. Emanuel and D. A. Raymond, pp. 181–184, Am. Meteor. Soc., Orlando, Fla.

Del Genio, A. D., M.-S. Yao, and J. Jonas (2007), Will moist convection be stronger in a warmer climate? *Geophys. Res. Lett.*, *34*, L16703, doi:10.1029/2007GL030525.

Del Genio, A. D., M.-S. Yao, W. Kovari, and K. K.-W. Lo (1996), A prognostic cloud water parameterization for global climate models. *J. Clim.*, *9*, 270–304, doi:10.1175/1520-0442(1996)009<0270:APCWPF>2.0.CO;2.

Donner, L. J., et al. (2011), The dynamical core, physical parameterizations, and basic simulation characteristics of the atmospheric component AM3 of the GFDL global coupled model CM3, *J. Clim.*, *24*, 3484–3519, doi:10.1175/2011JCLI3955.1.

Emanuel, A. K. (1991), A scheme for representing cumulus convection in large-scale models, *J. Atmos. Sci.*, *48*, 2313–2329, doi:10.1175/1520-0469(1991)048<2313:ASFRCC>2.0.CO;2.

Emanuel, A. K. (1993), A cumulus representation based on the episodic mixing model: the importance of mixing and microphysics in predicting humidity. *AMS Meteorol Monogr 24*(46), 185–192.

Endo, S., Y. Liu, W. Lin, and G. Liu (2011), Extension of WRF to cloud-resolving simulations driven by large-scale and surface forcings. Part I: Model configuration and validation, *Tech. Note BNL-96480-2011-JA*, Brookhaven Natl. Lab., New York. [Available at http://www.bnl.gov/envsci/pubs/pdf/2013/BNL-96480-2011-JA.pdf.].

Golaz, J.-C., V. E. Larson, and W. R. Cotton (2002a), A PDF-based model for boundary layer clouds. Part I: Method and model description, *J. Atmos. Sci.*, *59*, 3540–3551, doi:10.1175/1520-0469(2002)059<3540:APBMFB>2.0.CO;2.

Golaz, J.-C., V.E. Larson, W.R. Cotton (2002), A PDF-Based Model for Boundary Layer Clouds. Part II: Model Results. *J. Atmos. Sci.*, *59*, 3552–3571. doi: http://dx.doi.org/10.1175/1520-0469(2002)059<3552:APBMFB>2.0.CO;2.

Golaz, J.-C., V. E. Larson, J. A. Hansen, D. P. Schanen, and B. M. Griffin (2007), Elucidating model inadequacies in a cloud parameterization by use of an ensemble-based calibration framework, *Mon. Weather Rev.*, *135*, 4077–4096, doi:10.1175/2007MWR2008.1.

Grant, A. L. M. (2001), Cloud-base fluxes in the cumulus-capped boundary layer, *Q. J. R. Meteorol. Soc.*, *127*, 407–421.

Gregory, D., and P. R. R. Rowntree (1990), A mass flux convection scheme with representation of cloud ensemble characteristics and stability dependent closure, *Mon. Weather Rev.*, *118*, 1483–1506.

Hack, J. J. (1994), Parameterization of moist convection in the National Center for Atmospheric Research community climate model (CCM2), *J. Geophys. Res.*, *99*, 5551–5568.

Heus, T., et al. (2010), Formulation of the Dutch atmospheric large-eddy simulation (DALES) and overview of its applications, *Geosci. Model Dev.*, *3*, 415–444, doi:10.5194/gmd-3-415-2010.

Hewitt, H. T., D. Copsey, I. D. Culverwell, C. M. Harris, R. S. R. Hill, A. B. Keen, A. J. McLaren, and E. C. Hunke (2011), Design and implementation of the infrastructure of HadGEM3: The next generation Met Office climate modelling system, *Geosci. Model Dev.*, *4*, 223–253.

Holtslag, A. A. M., and B. A. Boville (1993), Local versus nonlocal boundary-layer diffusion in a global climate model, *J. Clim.*, *6*, 1825–1842, doi:10.1175/1520-0442(1993)006<1825:LVNBLD>2.0.CO;2.

Holtslag, A. A. M., and C.-H. Moeng (1991), Eddy diffusivity and countergradient transport in the convective atmospheric boundary layer, *J. Atmos. Sci.*, *48*, 1690–1698, doi:10.1175/1520-0469(1991)048<1690:EDACTI>2.0.CO;2.

Hourdin, F., et al. (2006), The LMDZ4 general circulation model: Climate performance and sensitivity to parametrized physics with emphasis on tropical convection, *Clim. Dyn.*, *27*(7), 787–813.

Isotta, F. A., P. Spichtinger, U. Lohmann, and K. von Salzen (2011), Improvement and implementation of a parameterization for shallow cumulus in the global climate model ECHAM5-HAM, *J. Atmos. Sci.*, *68*, 515–532.

JMA (2013), Outline of the operational numerical weather prediction at the Japan Meteorological Agency, Appendix to WMO *Tech. Prog. Rep. on the Global Data-Processing and Forecasting System and Numerical Weather Prediction Research*, Jpn. Meteorol. Agency, Tokyo. [Available at http://www.jma.go.jp/jma/jma-eng/jma-center/nwp/outline2013-nwp/index.htm.].

Kato, S., et al. (2011), Improvements of top-of-atmosphere and surface irradiance computations with CALIPSO, CloudSat, and MODIS-derived cloud and aerosol properties, *J. Geophys. Res.*, *116*, D19209, doi:10.1029/2011JD016050.

Kawai, H. (2012), Examples of mechanisms for negative cloud feedback of stratocumulus and stratus in cloud parameterizations, *SOLA*, *8*, 150−154, doi:10.2151/sola.2012-037.

Khairoutdinov, M. F., and D. A. Randall (2003), Cloud-resolving modeling of the ARM summer 1997 IOP: Model formulation, results, uncertainties and sensitivities, *J. Atmos. Sci.*, *60*, 607–625.

Larson, V. E., and J.-C. Golaz (2005), Using probability density functions to derive consistent closure relationships among higher-order moments, *Mon. Weather Rev.*, *133*, 1023–1042.

Liepert, B. G., and M. Previdi (2012), Inter-model variability and biases of the global water cycle in CMIP3 coupled climate models, *Environ. Res. Lett.*, *7*, 014006, doi:10.1088/1748-9326/7/1/014006.

Lock, A. P. (2009), Factors influencing cloud area at the capping inversion for shallow cumulus clouds, *Q. J. R. Meteorol. Soc.*, *135*, 941–952, doi:10.1002/qj.424.

Lock, A. P., A. R. Brown, M. R. Bush, G. M. Martin, and R. N. B. Smith (2000), A new boundary layer mixing scheme. Part I: Scheme description and single-column model tests, *Mon. Weather Rev.*, *128*, 3187–3199, doi:10.1175/15200493(2000)128<3187:ANBLMS>2.0.CO;2.

Louis, J., and J. Geleyn (1982). A short history of the PBL parameterization at ECMWF. Proc. ECMWF Workshop on Planetary Boundary Layer Parameterization, *Reading, United Kingdom, ECMWF*, 59–80.

Ma, X., K. von Salzen, and J. Cole (2010), Constraints on first aerosol indirect effect from a combination of MODIS-CERES satellite data and global climate simulations, *Atmos. Chem. Phys.*, *10*, 9851–9861. [Available at http://www.doaj.org/doaj?func=openurl&genre=article&issn=16807367&date=2010&volume=10&issue=6&spage=13945.].

Martin, G. M., N. Bellouin, W. J. Collins, I. D. Culverwell, P. R. Halloran, S. C. Hardiman, T. J. Hinton, and C. D. Jones (2011), The HadGEM2 family of Met Office Unified Model climate configurations, *Geosci. Model Dev.*, *4*, 723–757, doi:10.5194/gmd-4-723-2011.

Mellor, G. L., and T. Yamada (1974), A hierarchy of turbulence closure models for planetary boundary layers, *J. Atmos. Sci.*, *31*, 1791–1806, doi:10.1175/1520-0469(1974)031<1791:AHOTCM>2.0.CO;2.

Mlawer, E. J., S. J. Taubman, P. D. Brown, M. J. Iacono, and S. A. Clough (1997), RRTM: A validated correlated-k model for the longwave, *J. Geophys. Res.*, *102*, 16,663–16,682.

Molod, A., L. Takacs, M. Suarez, J. Bacmeister, I-S. Song, A. Eichmann, Y. Chang (2012), The GEOS-5 Atmospheric General Circulation Model: Mean Climate and Development from MERRA to Fortuna. NASA Technical Report Series on Global Modeling and Data Assimilation, *NASA/TM-2008-104606*, *28*, 115.

Moorthi, S., and M. J. Suarez (1992), Relaxed Arakawa-Schubert: A parameterization of moist convection for general circulation models, *Mon. Weather Rev.*, *120*, 978–1002, doi:10.1175/1520-0493(1992)120<0978:RASAPO>2.0.CO;2.

Neale, R. B., et al. (2010), Description of the NCAR Community Atmospheric Model (CAM5.0), NCAR/TN 486+STR. [Available at http://www.cesm.ucar.edu/models/ccsm4.0/cam/docs/description/cam4_desc.pdf.].

Neale, R. B., et al. (2012), Description of the NCAR Community Atmospheric Model (CAM5.0), NCAR/TN 486+STR. [Available at http://www.cesm.ucar.edu/models/cesm1.0/cam/docs/description/cam5_desc.pdf.].

Neggers, R. A. J., M. Koehler, and A. A. M. Beljaars (2009a), A dual mass flux framework for boundary-layer convection. Part I: Transport, *J. Atmos. Sci.*, *66*, 1465–1487, doi:10.1175/2008JAS2635.1.

Neggers, R. A. J. (2009b), A dual mass flux framework for boundary-layer convection, Part II: Clouds, *J. Atmos. Sci.*, *66*, 1489–1506, doi:10.1175/2008JAS2636.1.

Pan, D.-M., and D. Randall (1998), A cumulus parameterization with a prognostic closure, *Q. J. R. Meteorol. Soc.*, *124*, 949–981.

Park, S., and C. S. Bretherton (2009), The University of Washington shallow convection and moist turbulence schemes and their impact on climate simulations with the community atmosphere model, *J. Clim.*, *22*, 3449–3469, doi:10.1175/2008JCLI2557.1.

Ramanathan, V., R. D. Cess, E. F. Harrison, P. Minnis, B. R. Barkstrom, and D. L. Hartmann (1989), Cloud-radiative forcing and climate: Results from the Earth Radiation Budget experiment, *Science*, *243*, 57–63.

Randall, D. A., and D. G. Cripe (1999), Alternative methods for specification of observed forcing in single-column models and cloud system models, *J. Geophys. Res.*, *104*(D20), 24,527–24,545, doi:10.1029/1999JD900765.

Randall, D. A., et al. (2007), Climate models and their evaluation, in *Climate Change 2007: The Scientific Basis*, edited by S. Solomon et al., pp. 589–662, Cambridge Univ. Press, Cambridge, U. K.

Rienecker, M.M., et al. (2008), The GEOS-5 Data Assimilation System Documentation of Versions 5.0.1 and 5.1.0, and 5.2.0. NASA Technical Report Series on Global Modeling and Data Assimilation, *NASA/TM-2008-104606*, *27*, 92.

Schmidt, G. A., et al. (2006), Present day atmospheric simulations using GISS ModelE: Comparison to in-situ, satellite and reanalysis data, *J. Clim.*, *19*, 153–192.

Siebesma, A. P., et al. (2004), Cloud representation in general circulation models over the northern Pacific Ocean: A EUROCS intercomparison study, *Q. J. R. Meteorol. Soc.*, *130*, 3245–3267.

Sobel, A., J. Nilsson, and L. Polvani (2001), The weak temperature gradient approximation and balanced tropical moisture waves, *J. Atmos. Sci.*, *58*, 3650–3665.

Soden, B. J., A. J. Broccoli, and R. S. Hemler (2004), On the use of cloud forcing to estimate cloud feedback, *J. Clim.*, *17*, 3661–3665.

Stevens, B., et al. (2005), Evaluation of large-eddy simulations via observations of nocturnal marine stratocumulus, *Mon. Weather Rev.*, *133*, 1443–1462.

Stevens, B., et al. (2013), The atmospheric component of the MPI-M earth system model: ECHAM6, *J. Adv. Model. Earth Syst.*, *5*, 146–172, doi:10.1002/jame.20015.

Stevens, B., and A. Seifert (2008), Understanding macrophysical outcomes of microphysical choices in simulations of shallow cumulus convection, *J. Meteorol. Soc. Jpn. A*, *86*, 143–162.

Teixeira, J., et al. (2011), Tropical and subtropical cloud transitions in weather and climate prediction models: The GCSS/WGNE Pacific cross-section intercomparison (GPCI), *J. Clim.*, *24*, 5223–5256, doi:10.1175/2011JCLI3672.1.

Tiedtke, M. (1989), A comprehensive mass flux scheme for cumulus parameterization in large-scale models, *Mon. Weather Rev.*, *117*, 1779–1800, doi:10.1175/1520-0493(1989)117<1779:ACMFSF>2.0.CO;2.

von Salzen, K., and N. A. McFarlane (2002), Parameterization of the bulk effects of lateral and cloud-top entrainment in transient shallow cumulus clouds, *J. Atmos. Sci.*, *59*, 1405–1430, doi:10.1175/1520-0469(2002)059<1405:POTBEO>2.0.CO;2.

von Salzen, K., et al. (2013), The Canadian Fourth Generation Atmospheric Global Climate Model (CanAM4). Part I: Representation of physical processes, *Atmosphere*, *51*, 104–125, doi:10.1080/07055900.2012.755610.

Webb, M. J., and A. Lock (2012), Coupling between subtropical cloud feedback and the local hydrological cycle in a climate model, *Clim. Dyn.*, *27*, 17–38, doi:10.1007/s00382-012-1608-5.

Xu, K.-M., and A. Cheng (2013), Evaluating low cloud simulation from an upgraded multiscale modeling framework. Part II: Seasonal variations over the Eastern Pacific, *J. Clim.*, *26*, 5741–5760, doi:10.1175/JCLI-D-12–00276.1.

Xu, K.-M., A. Cheng, and M. Zhang (2010), Cloud-resolving simulation of low-cloud feedback to an increase in sea surface temperature, *J. Atmos. Sci.*, *67*, 730–748.

Zelinka, M. D., S. A. Klein, and D. L. Hartmann (2012), Computing and partitioning cloud feedbacks using cloud property histograms. Part I: Cloud radiative kernels, *J. Clim.*, *25*, 3715–3735, doi:10.1175/JCLI-D-11-00248.1.

Zhang, M., and C. S. Bretherton (2008), Mechanisms of low cloud climate feedback in idealized single-column simulations with the Community Atmospheric Model (CAM3), *J. Clim.*, *21*, 4859–4878.

Zhang, M., et al. (2012), CGILS: An experimental design to study low cloud feedbacks in general circulation models by using single-column and large eddy simulation models, *J. Adv. Model. Earth Syst.*, *4*, M12001, doi:10.1029/2012MS000182.

Zhao, M., I. M. Held, S.-J. Lin, and G. A. Vecchi (2009), Simulations of global hurricane climatology, interannual variability, and response to global warming using a 50-km resolution GCM, *J. Clim.*, *22*, 6653–6678, doi:10.1175/2009JCLI3049.1.